Entangling two Dicke states in a periodic modulated quantum system

Wuji Zhang,[1] Ruifang Wu,[1] Chunfang Sun,[1] Chunfeng Wu,[2] and Gangcheng Wang[1,*]

[1]*Center for Quantum Sciences and School of Physics, Northeast Normal University, Changchun 130024, China*
[2]*Science, Mathematics and Technology, Singapore University of Technology and Design, 8 Somapah Road, Singapore 487372, Singapore*

We propose a theoretical approach for entangling two Dicke states in a periodic modulated quantum system. By considering two qubit ensembles that are nonuniformly coupled to a common resonator, we can derive an effective Hamiltonian whose energy levels depend nonlinearly on the excitation number of each qubit ensemble. A more simplified effective Hamiltonian can be obtained by selecting the appropriate driving parameters and initial state. Based on the dynamic evolution of the effective Hamiltonian, we can selectively achieve Dicke state transitions and generate entangled Dicke states controllably. For a special case, we can obtain ensemble-ensemble entangled states by performing a projective even-odd cat-state measurement. By implementing Gaussian soft temporal modulation, we can effectively suppress off-resonant contributions in the interaction and enhance the fidelity of target states. Furthermore, by utilizing the Holstein-Primakoff transformation, we study the resonator-ensemble coupling system in the thermodynamic limit and investigate the generation of entangled magnon states. Additionally, we propose a scheme of creating magnon NOON states through frequency modulation and study the influence of decoherence on the fidelity of target states.

I. INTRODUCTION

Quantum entanglement, as a valuable resource for quantum information processing [1–6], has garnered significant attention due to its pivotal role in testing the fundamentals of quantum mechanics [7–10]. Recently, it has demonstrated a wide range of potential applications across various systems, encompassing atomic systems [11,12], photons [13–15], superconducting systems [16–21], trapped ions [22,23], and waveguides [24]. However, for large numbers of atoms, these schemes that rely on global control of the spin ensemble typically require intricate measurement-based feedback, high-fidelity control, and extensive preparation times, resulting in costly entangling gate operations between them [25–27]. Consequently, strategies for optimizing such schemes remain a significant challenge that requires attention [28].

Dicke states [29–31], originally introduced in the context of superradiance phenomenon [32,33], represent a special type of multiparticle entangled state. Due to their favorable properties, they hold promise for providing a reliable approach to address this issue in quantum sensing [34–37]. Compared with other states typically used in quantum sensing, Dicke states have been demonstrated to possess greater robustness to diverse sources of noise, such as qubit dephasing, qubit damping, and fluctuations in spin number [38–40]. It is noteworthy that utilizing entangled states has the potential to enhance measurement sensitivity beyond the standard quantum limit, in principle [41]. Considering the challenges involved in achieving precise control over individual spin qubits, global control over a collective of spins

facilitates the realization of optimal sensitivity through entangled Dicke states [42,43]. On the other hand, periodic driving has significant advantages in enhancing controllability of systems. This technique has been widely utilized in various areas of quantum physics, such as the investigation of exotic quantum phenomena in artificial materials [44], analysis of stochastic processes [45], Floquet engineering [46], and so on. Through periodic driving, one can effectively promote selective resonant transitions while suppressing undesired transitions within the targeted Hilbert subspace. As a result, a broad spectrum of controllable and selective interactions can be achieved, enabling enhanced controllability and selectivity [47].

The concept of selective interaction plays an important role in the preparation of controllable quantum entangled states [48–51]. This approach exploits the nonlinearity of energy levels to generate desired entangled states. In Refs. [47,52], the authors investigated the generation of Dicke states by means of selective interactions. By employing selective preparation of Dicke states, the initialization of a permutation-invariant quantum error-correction code was explored in Ref. [53]. This method facilitated the rapid generation of highly symmetric codes with exceptional fidelity. To realize the permutation-invariant quantum error-correction code, each logical qubit is encoded on several physical qubits. However, previous studies have paid little attention to methods for entangling states of two or several quantum systems in a controlled manner. A natural question arises regarding how to entangle logical qubits with selective interaction. This motivates us to delve into entanglement of multiple systems.

In this paper, we present a theoretical proposal for generating entangled Dicke states in the ultrastrong coupling regime. A series of unitary transformations have been applied to the

---

*wanggc887@nenu.edu.cn

013712-1

Hamiltonian to derive the effective interaction. Additionally, we investigate how to utilize selective resonant interactions to obtain entangled Dicke states in a finite system [54–58]. Furthermore, by utilizing the soft temporal quantum control, we can effectively mitigate unwanted off-resonant contributions. This approach allows for an accurate description of high-fidelity quantum states even in scenarios involving strong perturbations and long evolution times [59]. The collective operators can be mapped to Bosonic operators by means of Holstein-Primakoff transformation [60], thereby opening up an exciting possibility for employing the same approach to generate magnon NOON states.

This paper is structured as follows. In Sec. II, we derive the effective Hamiltonian by choosing appropriate unitary transformations. Section III presents a detailed scheme for generating entangled Dicke states with a high-fidelity quantum state using Gaussian soft control techniques. In Sec. IV, the Holstein-Primakoff transformation is utilized to establish selective interactions between two distinct magnons, thereby providing the potential for generating magnon NOON states in the thermodynamic limit. Furthermore, in Sec. V, we analyze the influence of decoherence on the dynamical evolution and evaluate the experimental feasibility of our proposed scheme. The results reveal that our approach can still achieve entangled target states with high fidelity. Finally, we draw our conclusions in Sec. VI.

II. THE EFFECTIVE HAMILTONIAN FOR FINITE QUBITS

We consider two qubit ensembles, each consisting of two-level systems, that are situated with a common quantum resonator. The jth ensemble comprising N_j qubits is coupled to the corresponding periodically driving field. The Hamiltonian is given by ($\hbar = 1$ throughout this work)

$$\hat{H} = \hat{H}_0 + \hat{H}_{\text{int}} + \hat{H}_d(t), \quad (1)$$

where

$$\hat{H}_0 = \omega_c \hat{a}^\dagger \hat{a} - \sum_{j=1}^{2} \varepsilon_j \hat{S}_j^z,$$

$$\hat{H}_{\text{int}} = \sum_{j=1}^{2} g_j(\hat{a} + \hat{a}^\dagger)\hat{S}_j^x,$$

$$\hat{H}_d(t) = \sum_{j=1}^{2} \left[\omega_{q_j} + A_j \cos(\omega t) \right] \hat{S}_j^x. \quad (2)$$

The notation $\hat{a}^\dagger$ ($\hat{a}$) denotes the creation (annihilation) operator of the cavity field with frequency ω_c, the notation ε_j is the atomic frequency in the jth ensemble, and g_j denotes the coupling strength between the resonator and qubits in the jth ensemble. The jth ensemble is subjected to a periodic driving field with amplitude A_j and frequency ω. The notation ω_{q_j} represents the static energy split of the biased term for the jth driving field. $\hat{S}_j^\alpha = \sum_{r_j=1}^{N_j} \hat{s}_{r_j}^\alpha$ ($\alpha = x, y, z$) are the collective operators with $\hat{s}_{r_j}^\alpha$ being the atomic operators acting on the r_jth site of the jth ensemble. We can verify that each ensemble operator satisfies the $\mathfrak{su}(2)$ algebra relations: $[\hat{S}_i^\alpha, \hat{S}_j^\beta] = i\delta_{ij}\epsilon_{\alpha\beta\gamma}\hat{S}_j^\gamma$ ($\alpha, \beta, \gamma \in \{x, y, z\}$), with δ_{ij} and $\epsilon_{\alpha\beta\gamma}$ being the

Kronecker delta and Levi-Civita symbols. To achieve a better understanding of the system, we apply the following unitary transformation:

$$\hat{U} = \exp\left[\sum_{j=1}^{2} \frac{g_j}{\omega_c} (\hat{a} - \hat{a}^\dagger)\hat{S}_j^x \right] \times \exp\left[i\frac{\pi}{\sqrt{2}} \sum_{j=1}^{2} \left(\hat{S}_j^x + \hat{S}_j^z \right) \right].$$

The transformed Hamiltonian can be expressed as

$$\hat{H}'(t) = \hat{U}^\dagger \hat{H} \hat{U} = \hat{H}_0'(t) + \hat{H}_{\text{int}}', \quad (3)$$

where

$$\hat{H}_0'(t) = \omega_c \hat{a}^\dagger \hat{a} + \hat{F}\left(\hat{S}_1^z, \hat{S}_2^z \right) + \sum_{j=1}^{2} A_j \cos(\omega t)\hat{S}_j^z,$$

$$\hat{H}_{\text{int}}' = -\sum_{j=1}^{2} \frac{\varepsilon_j}{2} [\hat{D}(\beta_j)\hat{S}_j^+ + \hat{D}^\dagger(\beta_j)\hat{S}_j^-],$$

where $\hat{D}(\beta_j) = \exp(\beta_j \hat{a}^\dagger - \beta_j^* \hat{a})$ is the displacement operator with $\beta_j = g_j/\omega_c$, and

$$\hat{F}(\hat{S}_1^z, \hat{S}_2^z) = \sum_{j=1}^{2} \omega_{q_j} \hat{S}_j^z - \omega_c \sum_{j=1}^{2} \left(\beta_j \hat{S}_j^z \right)^2 - 2\frac{g_1 g_2}{\omega_c} \hat{S}_1^z \hat{S}_2^z.$$

Moving to the rotating frame defined by

$$\hat{U}_0(t) = \exp\left[-i \int_0^t d\tau \hat{H}_0'(\tau) \right], \quad (4)$$

we further obtain the following transformed Hamiltonian [61]:

$$\hat{H}_I'(t) = -\sum_{j=1}^{2} \frac{\varepsilon_j}{2} [\hat{D}(\beta_j e^{i\omega_c t})\hat{S}_j^+ e^{i\eta_j \sin(\omega t)} e^{i\hat{f}_j(\hat{S}_1^z, \hat{S}_2^z)t} + \text{H.c.}], \quad (5)$$

where

$$\hat{f}_1(\hat{S}_1^z, \hat{S}_2^z) = \hat{F}\left(\hat{S}_1^z + 1, \hat{S}_2^z \right) - \hat{F}\left(\hat{S}_1^z, \hat{S}_2^z \right)$$

$$= \omega_{q_1} - \frac{2g_1 g_2}{\omega_c} \hat{S}_2^z - \frac{g_1^2}{\omega_c} \left(2\hat{S}_1^z + 1 \right),$$

$$\hat{f}_2(\hat{S}_1^z, \hat{S}_2^z) = \hat{F}\left(\hat{S}_1^z, \hat{S}_2^z + 1 \right) - \hat{F}\left(\hat{S}_1^z, \hat{S}_2^z \right)$$

$$= \omega_{q_2} - \frac{2g_1 g_2}{\omega_c} \hat{S}_1^z - \frac{g_2^2}{\omega_c} \left(2\hat{S}_2^z + 1 \right).$$

Utilizing the Jacobi-Anger identity [62]

$$e^{i\eta_j \sin(\omega t)} = \sum_{q=-\infty}^{\infty} \mathcal{J}_q(\eta_j) e^{iq\omega t}, \quad (6)$$

with $\mathcal{J}_q(\eta_j)$ being the qth order Bessel function of the first kind with $\eta_j = A_j/\omega$, the Hamiltonian in Eq. (5) can be rewritten as

$$\hat{H}_I'(t) = -\sum_{q=-\infty}^{\infty}$$

$$\times \sum_{j=1}^{2} \left[\frac{\varepsilon_j}{2} \mathcal{J}_q(\eta_j)\hat{D}[\beta_j(t)]\hat{S}_j^+ e^{i[q\omega + \hat{f}_j(\hat{S}_1^z, \hat{S}_2^z)]t} + \text{H.c.} \right], \quad (7)$$

where $\beta_j(t) = \beta_j e^{i\omega_c t}$. Since the Hamiltonian is permutation symmetric for each qubit ensemble, we introduce the following normalized N_j-qubit Dicke states with k_j atomic excitations for convenience [63,64]:

$$|W_{N_j}^{k_j}\rangle = (C_{k_j}^{N_j})^{-1/2} \sum_m P_m |e_1, e_2, \ldots, e_{k_j}, g_{k_j+1}, \ldots, g_{N_j}\rangle,$$

where $\sum_m P_m(\bullet)$ indicates the sum over all particle permutations for jth qubit ensembles and $C_{k_j}^{N_j} = N_j!/k_j!(N_j - k_j)!$ is the binomial coefficient. In the Dicke states basis, the collective operators can be reduced to the following $(N_j + 1)$-dimensional permutation symmetric subspace:

$$\hat{S}_j^z = \sum_{k_j=0}^{N_j} (k_j - \frac{N_j}{2}) |W_{N_j}^{k_j}\rangle\langle W_{N_j}^{k_j}|, \tag{8a}$$

$$\hat{S}_j^+ = \sum_{k_j=0}^{N_j} h_j(N_j, k_j) |W_{N_j}^{k_j+1}\rangle\langle W_{N_j}^{k_j}|, \tag{8b}$$

$$\hat{S}_j^- = \sum_{k_j=0}^{N_j} h_j(N_j, k_j) |W_{N_j}^{k_j}\rangle\langle W_{N_j}^{k_j+1}|, \tag{8c}$$

where $h_j(N_j, k_j) = \sqrt{(k_j + 1)(N_j - k_j)}$. In terms of the Fock state basis [47], the displacement operator can be rewritten as

$$\hat{D}[\beta_j(t)] = \sum_{m,n=0}^{\infty} \langle m|\hat{D}[\beta_j(t)]|n\rangle \hat{A}_{mn}, \tag{9}$$

where $\hat{A}_{m,n} = |m\rangle\langle n|$ and matrix elements $D_{mn}[\beta_j(t)] = \langle m|\hat{D}[\beta_j(t)]|n\rangle$ can be written as

$$D_{mn}[\beta_j(t)] = \begin{cases} e^{-\frac{1}{2}\beta_j^2} L_n^{(0)}(\beta_j^2), & m = n; \\ e^{-\frac{1}{2}\beta_j^2} \beta_j^s e^{is\omega_c t} \sqrt{\frac{n!}{m!}} L_n^{(s)}(\beta_j^2), & m > n; \\ e^{-\frac{1}{2}\beta_j^2} (-\beta_j)^s e^{-is\omega_c t} \sqrt{\frac{m!}{n!}} L_m^{(s)}(\beta_j^2), & m < n. \end{cases}$$

Here, $L_n^{(s)}(\beta_j^2)$ is an associated Laguerre polynomial with $s = |m - n|$. The cases $s = 0$ and $s > 0$ correspond to carrier transition and the sth sidebands transition, respectively. In terms of Dicke states and Fock states, the Hamiltonian in Eq. (7) can be reduced to the following Dicke state subspace:

$$\hat{H}_I'(t) = \hat{H}_{car}(t) + \hat{H}_{red}(t) + \hat{H}_{blue}(t), \tag{10}$$

where

$$\hat{H}_{car}(t) = \sum_{n=0}^{\infty} \sum_{k_1,k_2} \left[G_1^{(0)}(k_1, \eta_1) e^{i\delta_1^{(0)}t} \hat{W}_{N_1}^{k_1+1,k_1} \otimes \hat{W}_{N_2}^{k_2,k_2} \otimes \hat{A}_{n,n} + G_2^{(0)}(k_2, \eta_2) e^{i\delta_2^{(0)}t} \hat{W}_{N_1}^{k_1,k_1} \otimes \hat{W}_{N_2}^{k_2+1,k_2} \otimes \hat{A}_{n,n} \right] + \text{H.c.},$$

$$\hat{H}_{red}(t) = \sum_{n=0}^{\infty} \sum_{s=1}^{\infty} \sum_{k_1,k_2} \left[G_1^{(s)}(k_1, \eta_1) e^{i\delta_1^{(s)}t} \hat{W}_{N_1}^{k_1+1,k_1} \otimes \hat{W}_{N_2}^{k_2,k_2} \otimes \hat{A}_{n+s,n} + G_2^{(s)}(k_2, \eta_2) e^{i\delta_2^{(s)}t} \hat{W}_{N_1}^{k_1,k_1} \otimes \hat{W}_{N_2}^{k_2+1,k_2} \otimes \hat{A}_{n+s,n} \right] + \text{H.c.},$$

$$\hat{H}_{blue}(t) = \sum_{n=0}^{\infty} \sum_{s=1}^{\infty} \sum_{k_1,k_2} \left[(-1)^s G_1^{(s)}(k_1, \eta_1) e^{i\delta_1^{(-s)}t} \hat{W}_{N_1}^{k_1+1,k_1} \otimes \hat{W}_{N_2}^{k_2,k_2} \otimes \hat{A}_{n,n+s} \right.$$
$$\left. + (-1)^s G_2^{(s)}(k_2, \eta_2) e^{i\delta_2^{(-s)}t} \hat{W}_{N_1}^{k_1,k_1} \otimes \hat{W}_{N_2}^{k_2,k_2+1} \otimes \hat{A}_{n,n+s} \right] + \text{H.c..} \tag{11}$$

Here, $\hat{W}_{N_j}^{k_j,k_j'} = |W_{N_j}^{k_j}\rangle\langle W_{N_j}^{k_j'}|$ and $G_j^{(s)}(k_j, \eta_j) = -\frac{1}{2}\varepsilon_j \mathcal{J}_q(\eta_j) h_j(N_j, k_j) D_{mn}(\beta_j)$, with $\delta_j^{(\pm s)} = q\omega + \Delta_j \pm s\omega_c$ and

$$\Delta_1(k_1, k_2) = \omega_{q_1} + \frac{g_1^2}{\omega_c}(N_1 - 2k_1 - 1) + \frac{g_1 g_2}{\omega_c}(N_2 - 2k_2),$$

$$\Delta_2(k_1, k_2) = \omega_{q_2} + \frac{g_2^2}{\omega_c}(N_2 - 2k_2 - 1) + \frac{g_1 g_2}{\omega_c}(N_1 - 2k_1).$$

Obviously, we can tune the driving parameters to obtain the desired effective Hamiltonians. If the driving frequency $\omega = -\Delta_1(k_1, k_2)/q_0$, $-\Delta_1(k_1 - 1, k_2)/q_0$, $-\Delta_2(k_1, k_2)/q_0$, or $-\Delta_2(k_1, k_2 - 1)/q_0$, the on-resonance terms only appear in the carrier terms [i.e., $\hat{H}_{car}(t)$ in Eq. (10)]. Neglecting the off-resonance terms in the expansion of the Hamiltonian $\hat{H}_I'(t)$, we can obtain the effective Hamiltonian based on the secular approximation [65]. Then, we can investigate the desired Dicke state transitions based on the selective interactions. Furthermore, assuming the initial state of the system is $|W_{N_1}^{k_1}\rangle \otimes |W_{N_2}^{k_2}\rangle \otimes |0\rangle$ under the new frame, we can verify that such an initial state corresponds to the following state in the original frame:

$$|W_{N_1}^{k_1}\rangle_x \otimes |W_{N_2}^{k_2}\rangle_x \otimes |\xi_{k_1,k_2}\rangle = \hat{U} |W_{N_1}^{k_1}\rangle \otimes |W_{N_2}^{k_2}\rangle \otimes |0\rangle, \tag{12}$$

where $|\xi_{k_1,k_2}\rangle = e^{-|\xi_{k_1,k_2}|^2/2} \sum_{n=0}^{\infty} (\xi_{k_1,k_2}^n/\sqrt{n!})|n\rangle$, with $\xi_{k_1,k_2} = (N_1/2 - k_1)\beta_1 + (N_2/2 - k_2)\beta_2$, and $\hat{U}$ is given by Eq. (3). In fact, $|W_{N_j}^{k_j}\rangle_x$ is also a Dicke state, such that $\hat{\mathbf{S}}_j^2|W_{N_j}^{k_j}\rangle_x = N_j/2(N_j/2 + 1)|W_{N_j}^{k_j}\rangle_x$ and $\hat{S}_j^x|W_{N_j}^{k_j}\rangle_x = (k_j - N_j/2)|W_{N_j}^{k_j}\rangle_x$. It is worth mentioning that if we consider the conditions $\epsilon_j \to 0$, $\omega_{q_j} > 0$ and without driving, the ground state in the frame associated with unitary transformation $\hat{U}$ is $|W_{N_1}^0\rangle \otimes |W_{N_2}^0\rangle \otimes |0\rangle$, which corresponds to the state $|W_{N_1}^0\rangle_x \otimes |W_{N_2}^0\rangle_x \otimes |\xi_{0,0}\rangle$ with $\xi_{0,0} = (N_1\beta_1 + N_2\beta_2)/2$ in the original frame. By tuning the driving frequency to satisfy the on-resonant condition and choosing the proper initial state, we can obtain a subspace spanned by involved states. For instance, if we tune the driving frequency $\omega = -\Delta_1(k_1, k_2)/q_0$ and choose $|W_{N_1}^{k_1}\rangle \otimes |W_{N_2}^{k_2}\rangle \otimes |0\rangle$ as the initial state, we can obtain the subspace spanned by $\{|W_{N_1}^{k_1}\rangle \otimes |W_{N_2}^{k_2}\rangle \otimes |0\rangle, |W_{N_1}^{k_1+1}\rangle \otimes |W_{N_2}^{k_2}\rangle \otimes |0\rangle\}$. For our choice, the carrier transition is activated and the
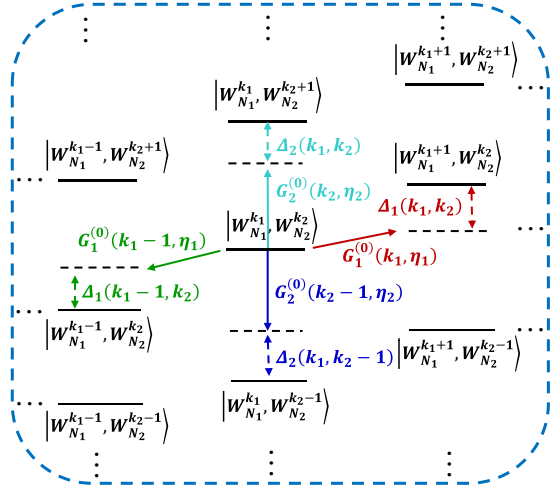
FIG. 1. Schematic diagram of transition, taking quantum state $|W_{N_1}^{k_1}, W_{N_2}^{k_2}\rangle$ as an example. Different driving Rabi frequencies $G_1^{(0)}(k_1, \eta_1)$ (solid magenta line), $G_1^{(0)}(k_1 - 1, \eta_1)$ (solid green line), $G_2^{(0)}(k_2, \eta_2)$ (solid blue line), and $G_2^{(0)}(k_2 - 1, \eta_2)$ (solid cyan line) close to resonant transition result in selective transitions.

field part of the state remains on the "vacuum" state. Considering this is such a special case, we will omit it in the following discussions and hereafter study the generation of Dicke states in the new frame for simplicity, unless specified otherwise. The transition diagram for two Dicke states is displayed in Fig. 1. In this figure, we choose quantum state $|W_{N_1}^{k_1}, W_{N_2}^{k_2}\rangle$ ($|W_{N_1}^{k_1}, W_{N_2}^{k_2}\rangle \equiv |W_{N_1}^{k_1}\rangle \otimes |W_{N_2}^{k_2}\rangle$) to be the initial state as an example. Driving a carrier transition close to resonance results in different effective interactions. Based on these properties, we can realize the so-called selective interactions, which allows to entangle two Dicke states by tuning the desired driving parameters.

The terms of $\hat{W}_{N_1}^{k_1'+1, k_1'} \otimes \hat{W}_{N_2}^{k_2', k_2'}$ and its Hermitian are time independent only when the driving frequency $\omega = -\Delta_1(k_1', k_2')/q_0$ is tuned. To safely disregard the impact of nonresonant terms within the effective Hamiltonian, it is necessary to satisfy the rotating wave approximation (RWA) condition, which effectively suppresses undesired transitions. Therefore, the conditions $|q\omega + \Delta_2(k_1, k_2)| \gg |G_2^{(0)}(k_2, \eta_2)|$ and $|q\omega + \Delta_1(k_1, k_2)| \gg |G_1^{(0)}(k_1, \eta_1)|$ for $k_1 \neq k_1'$ or $k_2 \neq k_2'$ or $q \neq q_0$ need to be fulfilled within the ultrastrong coupling regime. According to the constraint, only the transition $|W_{N_1}^{k_1'}, W_{N_2}^{k_2'}\rangle \leftrightarrow |W_{N_1}^{k_1'+1}, W_{N_2}^{k_2'}\rangle$ is possible, and the other transitions are not permitted. In this case, the effective Hamiltonian is given as

$$\hat{H}_{\text{eff}}^{(1)} = G_1^{(0)}(k_1', \eta_1)\big[\hat{W}_{N_1}^{k_1'+1, k_1'} \otimes \hat{W}_{N_2}^{k_2', k_2'} + \text{H.c.}\big]. \quad (13)$$

The terms of $\hat{W}_{N_1}^{k_1', k_1'} \otimes \hat{W}_{N_2}^{k_2'+1, k_2'}$ and its Hermitian are time independent only when the driving frequency reaches the resonance condition $\omega = -\Delta_2(k_1', k_2')/q_0$. Similarly, the conditions $|q\omega + \Delta_1(k_1, k_2)| \gg |G_1^{(0)}(k_1, \eta_1)|$ and $|q\omega + \Delta_2(k_1, k_2)| \gg |G_2^{(0)}(k_2, \eta_2)|$ for $k_1 \neq k_1'$ or $k_2 \neq k_2'$ or $q \neq q_0$ need to be satisfied in the ultrastrong coupling regime. Under these circumstances, only the transition $|W_{N_1}^{k_1'}, W_{N_2}^{k_2'}\rangle \leftrightarrow |W_{N_1}^{k_1'}, W_{N_2}^{k_2'+1}\rangle$ is permitted, and other transitions are forbidden. Accordingly, the effective Hamiltonian
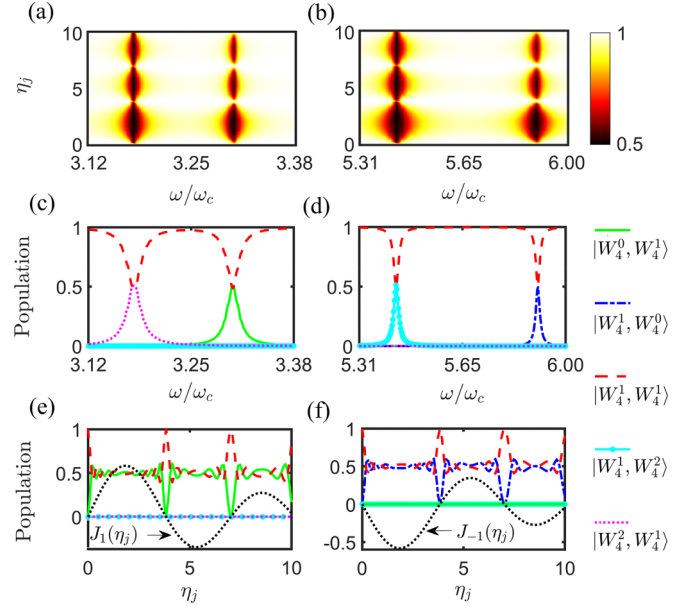

FIG. 2. Numerical results of the entangled Dicke states based on the selective resonant interaction. [(a) and (b)] Average population of initial state $|W_4^1, W_4^1\rangle$ as the function of driving frequency ω and parameter η_j. [(c) and (d)] Population transferred from the initial state $|W_4^1, W_4^1\rangle$ to the Dicke states $|W_4^1, W_4^0\rangle$, $|W_4^0, W_4^1\rangle$, $|W_4^2, W_4^1\rangle$, and $|W_4^1, W_4^2\rangle$ as the function of ω/ω_c at the fixed parameter $\eta_j = 1.09$. [(e) and (f)] Population from the initial state $|W_4^1, W_4^1\rangle$ to the Dicke states $|W_4^0, W_4^1\rangle$ and $|W_4^1, W_4^0\rangle$ at the fixed driving parameter $\omega = 3.3025$ or 5.9053. The dynamics is governed by the Hamiltonian in Eq. (2). The other parameters are chosen as $\omega_c/2\pi = 2.2$ GHz, $g_1 = 0.25\omega_c$, $g_2 = 0.49\omega_c$, $\varepsilon_1 = \varepsilon_2 = 0.01\omega_c$, $\omega_{q_1} = 2.87\omega_c$, and $\omega_{q_2} = 4.94\omega_c$.

reads

$$\hat{H}_{\text{eff}}^{(2)} = G_2^{(0)}(k_2', \eta_2)\big[\hat{W}_{N_1}^{k_1', k_1'} \otimes \hat{W}_{N_2}^{k_2'+1, k_2'} + \text{H.c.}\big]. \quad (14)$$

Based on the conditions described above, we can achieve the desired transition between the initial and final states. In the following section, we will explore the applications of the so-called selective interactions.

III. THE APPLICATIONS OF SELECTIVE TRANSITION

A. Selective interaction dynamics in two qubit ensembles

Through the implementation of controllable interactions, we possess the capability to generate a wide range of entangled Dicke states. To illustrate selective transitions, we will explain how to achieve the desired state in a specific example. Considering that each ensemble constitutes four qubits (i.e., $N_1 = N_2 = 4$, $q_0 = -1$) with the initial state $|W_4^1, W_4^1\rangle$, one can selectively obtain various final states such as $|W_4^1, W_4^0\rangle$, $|W_4^0, W_4^1\rangle$, $|W_4^2, W_4^1\rangle$, and $|W_4^1, W_4^2\rangle$. With the mechanism of the dominated role of the selective interaction in the dynamics of the system at hand, we have shown the calculated time-averaged population: $\overline{P} = \frac{1}{T}\int_0^T |\langle\beta|\psi(t)\rangle|^2 dt$ with $|\beta\rangle = |W_4^1, W_4^1\rangle$ as a function of the modulation frequency and modulation index in Fig. 2. In the regime of high modulation frequency ($\omega \gg G_j^{(0)}$), the dynamics is relatively robust and dictated by the Bessel functions. It
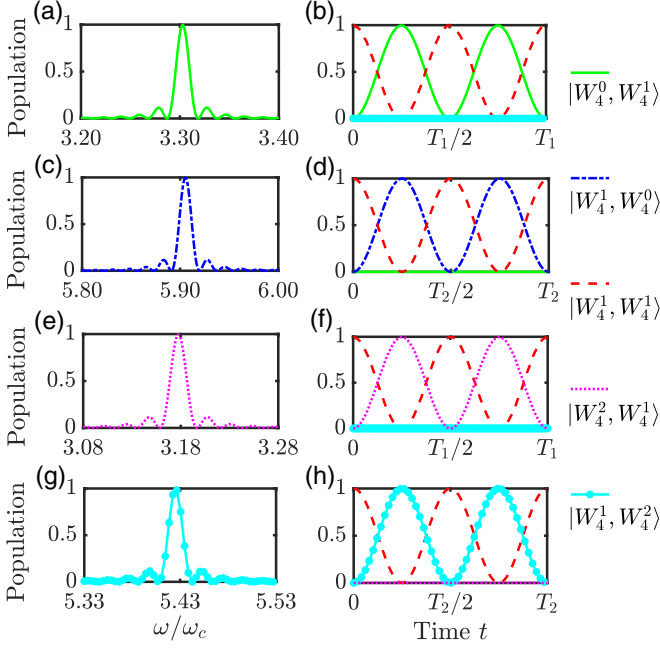
FIG. 3. Numerical results of the dynamics evolution based on the selective resonant interaction. [(a), (c), (e), and (g)] Population of the states $|W_4^0, W_4^1\rangle$, $|W_4^1, W_4^0\rangle$, $|W_4^2, W_4^1\rangle$, and $|W_4^1, W_4^2\rangle$ generated from $|W_4^1, W_4^1\rangle$ versus ω/ω_c. [(b), (d), (f), and (h)] Dynamics evolution of the Dicke states $|W_4^0, W_4^1\rangle$, $|W_4^1, W_4^0\rangle$, $|W_4^2, W_4^1\rangle$, and $|W_4^1, W_4^2\rangle$ generated from $|W_4^1, W_4^1\rangle$ versus time t. The dynamics is governed by the Hamiltonian in Eq. (2). The other parameters are chosen as $\eta_1 = \eta_2 = 1.09$, $\omega_c/2\pi = 2.2$ GHz, $g_1 = 0.25\omega_c$, $g_2 = 0.49\omega_c$, $\varepsilon_1 = \varepsilon_2 = 0.01\omega_c$, $\omega_{q_1} = 2.87\omega_c$, and $\omega_{q_2} = 4.94\omega_c$.

FIG. 4. The population of entangled Dicke state for $N_1 = N_2 = 4$ from $(|W_4^4, W_4^0\rangle + |W_4^0, W_4^4\rangle)/\sqrt{2}$ versus time t. The dynamics is governed by the Hamiltonian in Eq. (2). The other parameters are chosen as $\eta_1 = \eta_2 = 0.18$, $\omega_c/2\pi = 2.2$ GHz, $g_1 = 0.25\omega_c$, $g_2 = 0.49\omega_c$, $\varepsilon_1 = \varepsilon_2 = 0.01\omega_c$, $\omega_{q_1} = 2.87\omega_c$, and $\omega_{q_2} = 4.94\omega_c$.

can be easily seen that the pearl stripes align along the η_j axis at resonances, while the local minima along the chains indicate the values of η_j at which population trapping takes place. Between the stripes (along the ω/ω_c axis), the average population of $|W_4^1, W_4^1\rangle$ remains due to the atoms being driven far off-resonance. In Figs. 2(c) and 2(d), we further show how the population of each quantum state changes with the driving frequency, while assuming a fixed value for the parameter η_j. The resonances can be identified at the intersection of peaks and dips. Once the resonance condition is satisfied, the population dynamics exhibits coherent Rabi oscillations at those peaks. Far away from the resonances, the system has a small probability of evolution due to the off-resonance. We also note that the effective Rabi coupling is directly proportional to $\mathcal{J}_q(\eta_j)$. Consequently, at the zeros of Bessel function [$\mathcal{J}_q(\eta_j) = 0$], the dynamics freezes and leads to population trapping [66]. In Figs. 2(e) and 2(f), we show the results for the case of resonances, and the peaks appear at the zeros of $\mathcal{J}_q(\eta_j) = 0$. We find that the dynamical evolution is switched off and the corresponding transition is strongly suppressed. Through an appropriate choice of η_j, we observe either population trapping or coherent dynamics between the initial state and final states. In short, an invariant population at the driving-induced resonance indicates the population trapping.

For highlighting the nonlinearity of energy level and characteristic selective transitions, a comprehensive analysis of both Figs. 2 and 3 reveals that assuming the driving frequency
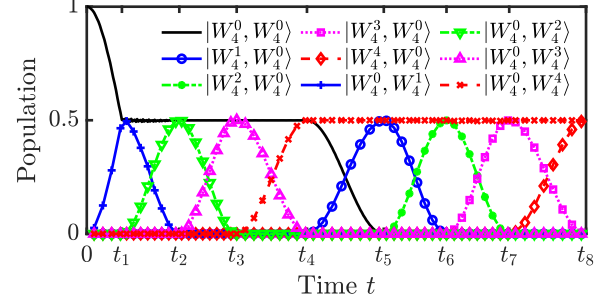
$\omega = \Delta_1(0, 1) = 3.3025\omega_c$, the Rabi oscillation between $|W_4^1, W_4^1\rangle$ and $|W_4^0, W_4^1\rangle$ can be obtained with a period of approximately $T_1 = 2\pi/[G_1^{(0)}(0, 1.09)] \approx 0.1002\,\mu s$. Similarly, we can manipulate the driving frequency $\omega = \Delta_2(1, 0) = 5.9053\omega_c$ to achieve the evolution state from $|W_4^1, W_4^1\rangle$ to $|W_4^1, W_4^0\rangle$ with the time period of $T_2 = 2\pi/[G_2^{(0)}(0, 1.09)] \approx 0.1095\,\mu s$. Furthermore, when the driving frequency $\omega = \Delta_1(1, 1) = 3.1775\omega_c$, the evolution of the system leads to the population transfer from $|W_4^1, W_4^1\rangle$ to $|W_4^2, W_4^1\rangle$ with the period of $T_1 = 2\pi/[G_1^{(0)}(1, 1.09)] \approx 0.0818\,\mu s$. While adjusting the driving frequency $\omega = \Delta_2(1, 1) = 5.4251\omega_c$, the Hamiltonian in Eq. (2) results in the creation of the quantum state $|W_4^1\rangle \otimes |W_4^2\rangle$ with the time period of $T_2 = 2\pi/[G_2^{(0)}(1, 1.09)] \approx 0.0894\,\mu s$.

B. Generation of entangled Dicke states

In terms of implementing the controllable interaction, it is also possible to achieve the desired entangled Dicke states through a multistep process. Here, we present an example of entangling two Dicke states by desired interaction. The target state reads

$$|\psi(t_f)\rangle = \frac{1}{\sqrt{2}}\left(|W_4^4, W_4^0\rangle + |W_4^0, W_4^4\rangle\right). \quad (15)$$

The corresponding dynamic evolution process is shown in Fig. 4. We will provide a detailed, step-by-step explanation of how to achieve the target state.

(1) Initially, we prepare the entire system in the state $|\psi(t_0)\rangle = |W_4^0, W_4^0\rangle$. Applying the resonance Hamiltonian with the driving frequency $\omega = \Delta_1(0, 0)$ to ensure selective resonance between $|W_4^0, W_4^0\rangle$ and $|W_4^1, W_4^0\rangle$, we obtain the evolution state $|\psi(t_1)\rangle = (|W_4^0, W_4^0\rangle - i|W_4^1, W_4^0\rangle)/\sqrt{2}$ at time $t_1 = \pi/4\Omega_1^0 \approx 0.0654\,\mu s$ with $\Omega_1^0 \equiv G_1^{(0)}(0, 0.18)$.

(2) Specially, we set $\omega = \Delta_1(1, 0)$ to achieve the selective resonance between $|W_4^1, W_4^0\rangle$ and $|W_4^2, W_4^0\rangle$ as illustrated in Fig. 4. Then, the evolution state $|\psi(t_2)\rangle = (|W_4^0, W_4^0\rangle - |W_4^2, W_4^0\rangle)/\sqrt{2}$ after a period of time $t_2 = t_1 + \pi/2\Omega_2^0 \approx 0.1722\,\mu s$ with $\Omega_2^0 \equiv G_1^{(0)}(1, 0.18)$.

(3) Certainly, we can adjust $\omega = \Delta_1(2, 0)$ to hold perfect oscillations transition between $|W_4^2, W_4^0\rangle$ and $|W_4^3, W_4^0\rangle$. The

TABLE I. The generation of entangled Dicke state $(|W_4^4, W_4^0\rangle + |W_4^0, W_4^4\rangle)/\sqrt{2}$ with the initial state $|W_4^0, W_4^0\rangle$. The dynamics is governed by the Hamiltonian in Eq. (2).

Step l	Driving frequency ω/ω_c	Time duration (μs)	Final state for step l	Fidelity (abrupt)	Fidelity (soft)
1	3.5475	$\pi/4G_1^{(0)}(0, 0.18) \approx 0.0654$	$(|W_4^0, W_4^0\rangle - i|W_4^1, W_4^0\rangle)/\sqrt{2}$	0.9999	0.9999
2	3.4225	$\pi/2G_1^{(0)}(1, 0.18) \approx 0.1068$	$(|W_4^0, W_4^0\rangle - |W_4^2, W_4^0\rangle)/\sqrt{2}$	0.9989	0.9992
3	3.2975	$\pi/2G_1^{(0)}(2, 0.18) \approx 0.1068$	$(|W_4^0, W_4^0\rangle + i|W_4^3, W_4^0\rangle)/\sqrt{2}$	0.9954	0.9962
4	3.1725	$\pi/2G_1^{(0)}(3, 0.18) \approx 0.1308$	$(|W_4^0, W_4^0\rangle + |W_4^4, W_4^0\rangle)/\sqrt{2}$	0.9864	0.9918
5	6.1503	$\pi/2G_2^{(0)}(0, 0.18) \approx 0.0994$	$(|W_4^4, W_4^0\rangle - i|W_4^0, W_4^1\rangle)/\sqrt{2}$	0.9782	0.9877
6	5.6701	$\pi/2G_2^{(0)}(1, 0.18) \approx 0.0812$	$(|W_4^4, W_4^0\rangle - |W_4^0, W_4^2\rangle)/\sqrt{2}$	0.9700	0.9827
7	5.1899	$\pi/2G_2^{(0)}(2, 0.18) \approx 0.0812$	$(|W_4^4, W_4^0\rangle + i|W_4^0, W_4^3\rangle)/\sqrt{2}$	0.9409	0.9781
8	4.7097	$\pi/2G_2^{(0)}(3, 0.18) \approx 0.0994$	$(|W_4^4, W_4^0\rangle + |W_4^0, W_4^4\rangle)/\sqrt{2}$	0.9322	0.9624

resulting state is $|\psi(t_3)\rangle = (|W_4^0, W_4^0\rangle + i|W_4^3, W_4^0\rangle)/\sqrt{2}$ at time $t_3 = t_2 + \pi/2\Omega_3^0 \approx 0.2790$ μs with $\Omega_3^0 = G_1^{(0)}(2, 0.18)$.

(4) We tune $\omega = \Delta_1(3, 0)$ to attain the selective resonance between $|W_4^4, W_4^0\rangle$ and $|W_4^3, W_4^0\rangle$. The quantum state evolves into $|\psi(t_4)\rangle = (|W_4^0, W_4^0\rangle + |W_4^4, W_4^0\rangle)/\sqrt{2}$ at the moment $t_4 = t_3 + \pi/2\Omega_4^0 \approx 0.4098$ μs with $\Omega_4^0 \equiv G_1^{(0)}(3, 0.18)$.

(5) When the frequency $\omega = \Delta_2(0, 0)$ satisfies the condition of resonance, the evolved state changes into $|\psi(t_5)\rangle = (|W_4^4, W_4^0\rangle - i|W_4^0, W_4^1\rangle)/\sqrt{2}$ in the time $t_5 = t_4 + \pi/2\Omega_5^0 \approx 0.5092$ μs with $\Omega_5^0 = G_2^{(0)}(0, 0.18)$.

(6) Subsequently, we set $\omega = \Delta_2(0, 1)$ to maintain selective resonance almost strictly between the state $|W_4^0, W_4^1\rangle$ and $|W_4^0, W_4^2\rangle$. After $t_6 = t_5 + \pi/2\Omega_6^0 \approx 0.5904$ μs with $\Omega_6^0 = G_2^{(0)}(1, 0.18)$, the quantum state $|\psi(t_6)\rangle = (|W_4^4, W_4^0\rangle - |W_4^0, W_4^2\rangle)/\sqrt{2}$ can be realized.

(7) After applying the effective Hamiltonian $\hat{H}_{\text{eff}}^{(2)} = G_2^{(0)}(2, 0.28)[\hat{W}_4^{0,0} \otimes \hat{W}_4^{3,2} + \text{H.c.}]$ on the state $|\psi(t_6)\rangle$ and setting the driving frequency $\omega = \Delta_2(0, 2)$, we can reach the state $|\psi(t_7)\rangle = (|W_4^4, W_4^0\rangle + i|W_4^0, W_4^3\rangle)/\sqrt{2}$ at $t_7 = t_6 + \pi/2\Omega_7^0 \approx 0.6716$ μs with $\Omega_7^0 = G_2^{(0)}(2, 0.18)$.

(8) Finally, we tune the driving frequency $\omega = \Delta_2(0, 3)$ to derive the transition between $|W_4^0, W_4^3\rangle$ and $|W_4^0, W_4^4\rangle$. In the series of operations, the quantum state is excited to $|\psi(t_8)\rangle = (|W_4^4, W_4^0\rangle + |W_4^0, W_4^4\rangle)/\sqrt{2}$ at time $t_8 = t_7 + \pi/2\Omega_8^0 \approx 0.7709$ μs with $\Omega_8^0 = G_2^{(0)}(3, 0.18)$.

If all terms in Eq. (7) are fast-time varying, the higher-order effective Hamiltonian will dominate the dynamics [67]. Based on the higher-order Hamiltonian, the number of steps can be reduced. Tuning the driving frequency to obtain the two-atomic excitation process, we can reduce the eight-step operations to four-step operations [51]. The numerical results of the above eight-step protocol are listed in

Table I. The numerical simulation of the fidelity is defined as $F(|\psi_T\rangle, |\psi(t)\rangle) = |\langle \psi_T|\psi(t)\rangle|^2$, with $|\psi_T\rangle$ and $|\psi(t)\rangle$ being the target state and evolution state, respectively. Through the aforementioned procedure, we have successfully achieved the desired target state. The final state for the eighth step protocol reads

$$|\psi(t_8)\rangle = \frac{1}{\sqrt{2}}(|W_4^4, W_4^0\rangle + |W_4^0, W_4^4\rangle) \otimes |0\rangle. \quad (16)$$

In the original frame, such state can be recast as follows:

$$|\psi'(t_8)\rangle = \frac{1}{\sqrt{2}}(|W_4^4, W_4^0\rangle_x \otimes |\alpha\rangle + |W_4^0, W_4^4\rangle_x \otimes |-\alpha\rangle), \quad (17)$$

where $\alpha = 2(\beta_2 - \beta_1)$. Hence, we obtain the tripartite entangled states. Then, we will show how to obtain two entangled Dicke states based on projective measurement. The orthogonal even and odd Schrödinger cat states take the following form:

$$|C_\alpha^\pm\rangle = \mathcal{N}_\pm^{-1}(|\alpha\rangle \pm |-\alpha\rangle), \quad (18)$$

where $\mathcal{N}_\pm = \sqrt{2[1 \pm \exp(-2|\alpha|^2)]}$ are the respective normalization factors. Here, even or odd refers to the photon number of the cat states in Fock space, that is, a state containing only even or odd photon numbers. In terms of cat state basis, the final states can be rewritten as

$$|\psi'(t_8)\rangle = \frac{1}{2}[\mathcal{N}_+|D_x^+\rangle \otimes |C_\alpha^+\rangle + \mathcal{N}_-|D_x^-\rangle \otimes |C_\alpha^-\rangle], \quad (19)$$

where $|D_x^\pm\rangle = (|W_4^4, W_4^0\rangle_x \pm |W_4^0, W_4^4\rangle_x)/\sqrt{2}$ are entangled atomic Dicke states. Performing projective measurement on the system in the cat states basis [68], the atomic Dicke states can be derived. If the projective measurement result is even (odd) cat state $|C_\alpha^\pm\rangle$, we can obtain the atomic final states $|D_x^\pm\rangle$

TABLE II. The generation of magnon NOON state $(|2, 0\rangle + |0, 2\rangle)/\sqrt{2}$ with the initial state $|\psi(0)\rangle = |0, 0\rangle$. The dynamics is governed by the Hamiltonian in Eq. (24).

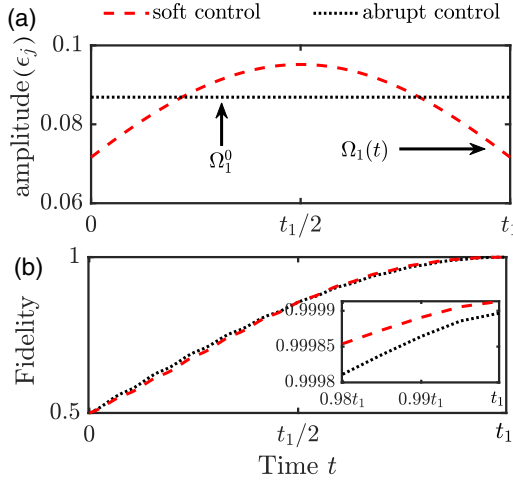| Step i	Driving frequency ω/ω_c	Time duration (μs)	Evolution state $|\psi(t_i)\rangle$	Fidelity (abrupt)	Fidelity (soft)
1	50.0900	$\pi/4G_{m1}^{(0)}(0, 0.12) \approx 0.0140$	$(|0, 0\rangle - i|1, 0\rangle)/\sqrt{2}$	0.9994	0.9999
2	49.9100	$\pi/2G_{m1}^{(0)}(0, 0.12) \approx 0.0198$	$(|0, 0\rangle - |2, 0\rangle)/\sqrt{2}$	0.9947	0.9998
3	82.1199	$\pi/2G_{m2}^{(0)}(0, 0.12) \approx 0.0302$	$(|2, 0\rangle - i|0, 1\rangle)/\sqrt{2}$	0.9846	0.9997
4	81.6397	$\pi/2G_{m2}^{(0)}(1, 0.12) \approx 0.0214$	$(|2, 0\rangle + |0, 2\rangle)/\sqrt{2}$	0.9715	0.9995

FIG. 5. (a) Abrupt driving and soft driving as a function of time t for step 1. (b) Fidelity of evolution state $(|W_4^0, W_4^0\rangle - i|W_4^1, W_4^0\rangle)/\sqrt{2}$ in step 1. Insets illustrate the fidelity of final state under both driving conditions. The dynamics is governed by the Hamiltonian in Eq. (2). The other parameters are chosen consistent with Fig. 4.

with probability $[1 \pm \exp(-2|\alpha|^2)]/2$. Hence, we obtain the entangled state for two qubit ensembles.

C. Fidelity enhancement via Gaussian soft quantum control

In Sec. III B, we assume that the drive is abruptly turned on at an initial time t_{l-1} and lasts till a final time t_l for the lth step. To improve the fidelity of the entangled Dicke states, we can employ Gaussian time-dependent control techniques, and achieve precise coupling to resonant terms through modulation of the coupling constant over time. The Gaussian soft control [59] offers the advantage of maintaining higher fidelity of the corresponding target quantum states within a broader parameter range, which accurately satisfy the conditions of RWA and avoid unnecessary transitions. Such temporal modulation significantly suppresses the nonresonant effects of the interaction while remaining insensitive to operation time, which can extremely improve the robustness of the scheme. Next, we change the time-independent Rabi frequency Ω_l^0 to a time-dependent Gaussian form [69]

$$\Omega_l(t) = \mu\Omega_l^0 \exp\left(-\frac{[t - (t_{l-1} + t_l)/2]^2}{2\sigma_l^2}\right), \quad (20)$$

where Ω_l^0 represents the corresponding Rabi frequency. t_{l-1} (t_l) is the minimum (maximum) of each segment evolution time in the eight-step operation. $\sqrt{2}\sigma_l$ is the width of the Gaussian pulse applied during each step of evolution. In order to maintain the necessary coherent process for the preparation of entangled states, the Gaussian pulses need to be satisfied,

$$A_l = \int_{t_{l-1}}^{t_l} \Omega_l(t)\,dt = \begin{cases} \frac{\pi}{4}, & \text{for step 1} \\ \frac{\pi}{2}, & \text{for other steps.} \end{cases} \quad (21)$$

According to Eq. (21), we have imposed a condition for calculating the pulse area within a finite time interval, ranging from t_{l-1} to t_l. This condition ensures that Gaussian pulses
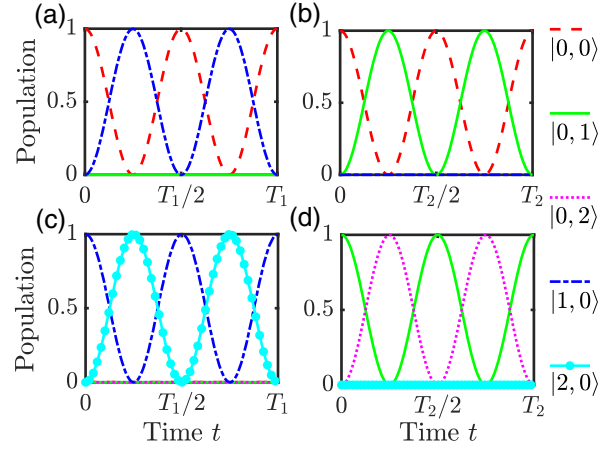

FIG. 6. (a)–(d) Populations with different magnon Fock states as the initial states. The dynamics is governed by the Hamiltonian in Eq. (24). The other parameters are chosen as $\eta_1 = \eta_2 = 0.12$, $\omega_c/2\pi = 2.2$ GHz, $g_1 = 0.30\omega_c$, $g_2 = 0.49\omega_c$, $\varepsilon_1 = \varepsilon_2 = 0.01\omega_c$, $\omega_{q_1} = 2.78\omega_c$, and $\omega_{q_2} = 4.94\omega_c$.

can be reliably substituted for the previous Rabi frequency Ω_l^0, i.e., $\mu > 1$. Furthermore, parameter σ_l is determined by the following relation:

$$\sigma_l = \frac{\sqrt{\pi}}{2\sqrt{2}n\mu\Omega_l(0)\text{erf}[(t_l - t_{l-1})/(2\sqrt{2}\sigma_l)]}. \quad (22)$$

Here, the function $\text{erf}(x) = \frac{2}{\sqrt{\pi}}\int_0^x dz e^{-z^2}$, and $n = 2$ for $l = 1$ and $n = 1$ for all other cases. We are able to achieve soft control by applying different Gaussian pulses to each step and then obtain high-fidelity target quantum states. In Fig. 5, we show the temporal evolution of both drive amplitudes in the initial state. Correspondingly, we present the fidelity of the desired target state throughout the evolution, with insets indicating that soft control yields a higher fidelity compared to abrupt control upon completion of the process. The situation can be explained as follows: when there is the absence of a modulation for $\Omega_l(t)$, i.e., abrupt driving Ω_l^0, unwanted terms in the effective Hamiltonian can be neglected by the RWA provided that the Δ_j is sufficiently large compared with Ω_l^0. However, after applying Gaussian soft control, we can calculate the Hamiltonian by using Mangus expansion for a time interval of $[t_{l-1}, t_l]$, where the mean coefficient $g_M \propto \mu\Omega_l^0 \exp(-\frac{1}{2}\sigma_l^2\Delta_j)$. A simple inspection of g_M reveals that the effective couplings decay exponentially with Δ_j at the fixed μ, and the contribution to the average Hamiltonian decreases accordingly. In other words, the high-frequency oscillation term can be greatly suppressed when the detuning amount is relatively large. In addition, we find that g_M is a monotonically increasing function with μ and larger g_M can have negative consequences on the coupling term of the resonance as the result of selecting a high value for μ. Thus, combined with practical implementations, it is essential to rationally choose μ to achieve high-fidelity quantum states. For the above consideration, we choose $\mu = \sqrt{6/5}$ to achieve soft control. The corresponding results, presented in the last column of Table I, show improvement in fidelity compared to abrupt control. So our soft control scheme enables highly

selective coupling between different resonance constituents of composite systems.

IV. THE THERMODYNAMIC LIMIT CASE

Now, we consider the effect of nonlinear energy levels in the thermodynamic limit ($N_1 \gg 1$ and $N_2 \gg 1$). With the Holstein-Primakoff transformation, the collective operators can be written as [60]

$$\hat{S}_j^z = \hat{m}_j^\dagger \hat{m}_j - s_j, \tag{23a}$$

$$\hat{S}_j^+ = \hat{m}_j^\dagger (2s_j - \hat{m}_j^\dagger \hat{m}_j)^{\frac{1}{2}}, \tag{23b}$$

$$\hat{S}_j^- = (2s_j - \hat{m}_j^\dagger \hat{m}_j)^{\frac{1}{2}} \hat{m}_j, \tag{23c}$$

where $s_j = N_j/2$ is the pseudospin quantum number for the jth qubit ensemble, and $\hat{m}_j^\dagger$ ($\hat{m}_j$) denotes the creation (annihilation) operator of the two different magnons. For the low-lying magnon excitations, i.e., $\langle \hat{m}_j^\dagger \hat{m}_j \rangle / 2s_j \ll 1$, we can safely approximate the collective operators as the following relations: $\hat{S}_j^+ \approx \sqrt{2s_j} \hat{m}_j^\dagger$, $\hat{S}_j^- \approx \sqrt{2s_j} \hat{m}_j$. Then, Eq. (7) reads

$$\hat{H}_I^m(t) = -\sum_{q=-\infty}^{\infty} \mathcal{J}_q(\eta_j) \left[\varepsilon_1 \sqrt{\frac{s_1}{2}} \hat{D}(\beta_1 e^{i\omega_c t}) \hat{m}_1^\dagger e^{i[q\omega + \Delta_1 + 2\frac{g_1 g_2}{\omega_c}(s_2 - \hat{m}_2^\dagger \hat{m}_2) + \frac{g_1^2}{\omega_c}(2s_1 - 2\hat{m}_1^\dagger \hat{m}_1 - 1)]t} \right.$$
$$\left. + \varepsilon_2 \sqrt{\frac{s_2}{2}} \hat{D}(\beta_2 e^{i\omega_c t}) \hat{m}_2^\dagger e^{i[q\omega + \Delta_2 + 2\frac{g_1 g_2}{\omega_c}(s_1 - \hat{m}_1^\dagger \hat{m}_1) + \frac{g_2^2}{\omega_c}(2s_2 - 2\hat{m}_2^\dagger \hat{m}_2 - 1)]t} + \text{H.c.} \right]. \tag{24}$$

In the subspace of two different magnon Fock states, the effective Hamiltonian (7) can be rewritten as

$$\hat{H}_I^m(t) = \sum_{q=-\infty}^{\infty} \sum_{m_1, m_2} \left[G_{m1}^{(0)}(m_1, \eta_1) e^{iq\omega t} e^{i\Delta_1(m_1, m_2)t} \hat{M}_{m_1+1, m_1} \otimes \hat{M}_{m_2, m_2} + G_{m2}^{(0)}(m_2, \eta_2) e^{iq\omega t} e^{i\Delta_2(m_1, m_2)t} \hat{M}_{m_1, m_1} \otimes \hat{M}_{m_2+1, m_2} + \text{H.c.} \right], \tag{25}$$

where m_j is the eigenvalue of the magnon Fock operator $\hat{m}_j^\dagger \hat{m}_j$, $\hat{M}_{m_j, m'_j} = |m_j\rangle\langle m'_j|$, $G_{mj}^{(0)}(m_j, \eta_j) = -\varepsilon_j \sqrt{s_j(m_j + 1)} \mathcal{J}_q(\eta_j) e^{-\frac{1}{2}\beta_j^2} / \sqrt{2}$, and

$$\Delta_1(m_1, m_2) = \Delta_1 + \frac{g_1^2}{\omega_c}(2s_1 - 2m_1 - 1) + 2\frac{g_1 g_2}{\omega_c}(s_2 - m_2),$$

$$\Delta_2(m_1, m_2) = \Delta_2 + \frac{g_2^2}{\omega_c}(2s_2 - 2m_2 - 1) + 2\frac{g_1 g_2}{\omega_c}(s_1 - m_1).$$

Similarly, in order to maintain the same approach as that mentioned above, we can tune the driving frequency ω to obtain the desired selective interactions based on the RWA. The terms of $\hat{M}_{m'_1+1, m'_1} \otimes \hat{M}_{m'_2, m'_2}$ and its Hermitian are time independent only when the driving frequency $\omega = -\Delta_1(m'_1, m'_2)/q_0$, if one can verify that the condition $|q\omega + \Delta_2(m_1, m_2)| \gg |G_{m2}^{(0)}(m_2, \eta_2)|$ holds to maintain for any q, m_1, and m_2. And, $|q\omega + \Delta_1(m_1, m_2)| \gg |G_{m1}^{(0)}(m_1, \eta_1)|$ for $m_1 \neq m'_1$ or $m_2 \neq m'_2$ or $q \neq q_0$ remains valid within the ultrastrong coupling regime. In this case, the transition occurs between $|m'_1, m'_2\rangle (|m'_1, m'_2\rangle \equiv |m'_1\rangle \otimes |m'_2\rangle)$ and $|m'_1 + 1, m'_2\rangle$, and the effective Hamiltonian reads

$$\hat{H}_{\text{eff}}^{(1)} = G_{m1}^{(0)}(m'_1, \eta_1)[\hat{M}_{m'_1+1, m'_1} \otimes \hat{M}_{m'_2, m'_2} + \text{H.c.}]. \tag{26}$$

The terms of $\hat{M}_{m'_1, m'_1} \otimes \hat{M}_{m'_2+1, m'_2}$ and its Hermitian are time independent only when the driving frequency is tuned $\omega = -\Delta_2(m'_1, m'_2)/q_0$, if we can ensure that the conditions $|q\omega + \Delta_1(m_1, m_2)| \gg |G_{m1}^{(0)}(m_1, \eta_1)|$ and $|q\omega + \Delta_2(m'_1, m'_2)| \gg |G_{m2}^{(0)}(m_2, \eta_2)|$ for $m_1 \neq m'_1$ or $m_2 \neq m'_2$ or $q \neq q_0$ are realized in the ultrastrong coupling regime. In such a case, the transition occurs between $|m'_1, m'_2\rangle$ and $|m'_1, m'_2 + 1\rangle$, and the effective Hamiltonian reads

$$\hat{H}_{\text{eff}}^{(2)} = G_{m2}^{(0)}(m'_2, \eta_2)[\hat{M}_{m'_1, m'_1} \otimes \hat{M}_{m'_2+1, m'_2} + \text{H.c.}]. \tag{27}$$

So far, the model Hamiltonian in the thermodynamic limit has been simplified as a controlled selective interaction under frequency modulation. Therefore, the applications of selective interactions can also be actualized under the thermodynamic limit.

For the sake of brevity, we focus on a system with a large number of qubits shown in Fig. 6, where the initial state $|\psi(0)\rangle = |0, 0\rangle$ with the total qubit number $N_1 = N_2 = 200$. Tuning the driving frequency $\omega = \Delta_1(0, 0)$, the transition of the quantum states between $|0, 0\rangle$ and $|1, 0\rangle$ can be achieved with a period of time $T_1 = 2\pi/[G_{m1}^{(0)}(0, 0.12)] \approx 0.1123 \,\mu s$. When the driving frequency is set to $\omega = \Delta_2(0, 0)$, we can derive the evolution state $|\psi(t)\rangle = \cos[G_{m2}^{(0)}(0, 0.12)t]|0, 0\rangle - i\sin[G_{m2}^{(0)}(0, 0, 12)t]|0, 1\rangle$ with a period of time $T_2 = 2\pi/[G_{m2}^{(0)}(0, 0.12)] \approx 0.1210 \,\mu s$. Similarly, supposing that the initial state is prepared as $|\psi(0)\rangle = |1, 0\rangle$, we obtain the transition of the quantum states between $|1, 0\rangle$ and $|2, 0\rangle$ by tuning the driving frequency $\omega = \Delta_1(1, 0)$ with a period of time $T_1 = 2\pi/[G_{m1}^{(0)}(1, 0.12)] \approx 0.0794 \,\mu s$. Taking into account $|\psi(0)\rangle = |0, 1\rangle$ as the initial state, the transition of the quantum state between $|0, 1\rangle$ and $|0, 2\rangle$ can be obtained with a period of time $T_2 = 2\pi/[G_{m2}^{(0)}(1, 0.12)] \approx 0.0856 \,\mu s$ by adjusting the driving frequency $\omega = \Delta_2(0, 1)$.

In the following, we will show how to prepare the magnon NOON states with selective resonance interaction. This is clearly illustrated in Fig. 7 and detailed data is given in Table II. If the magnons are not initially distributed throughout the system, the initial state can be expressed as $|\psi(0)\rangle = |0, 0\rangle$. By tuning the driving frequency $\omega = \Delta_1(0, 0)$, the evolved state is $|\psi(t_1)\rangle = (|0, 0\rangle - i|1, 0\rangle)/\sqrt{2}$ after a duration of $t_1 = \pi/4G_{m1}^{(0)}(0, 0.12) \approx 0.0140 \,\mu s$. Again adjusting the driving frequency $\omega = \Delta_1(1, 0)$, the evolved state can be expressed as $|\psi(t_2)\rangle = (|0, 0\rangle - |2, 0\rangle)/\sqrt{2}$ at the time $t_2 =$
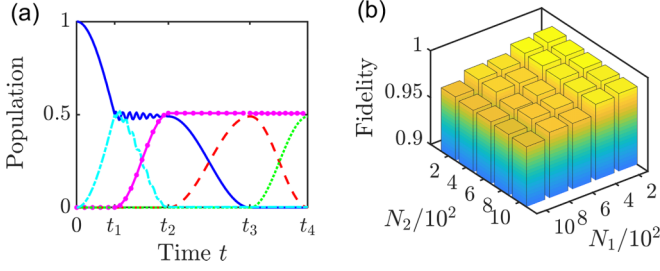
FIG. 7. (a) Populations of the magnon NOON states from $|0,0\rangle$ versus time t. Evolution states $|0,0\rangle$ (solid cyan line), $(|0,0\rangle - i|1,0\rangle)/\sqrt{2}$ (dotted blue line), $(|0,0\rangle - |2,0\rangle)/\sqrt{2}$ (dotted magenta line), $(|2,0\rangle - i|0,1\rangle)/\sqrt{2}$ (dotted red line), and $(|2,0\rangle + |0,2\rangle)/\sqrt{2}$ (dotted green line). (b) Fidelity with choosing different total qubit number N_1 and N_2 for generating magnon NOON states. The dynamics is governed by the Hamiltonian in Eq. (24). The parameters are chosen as $\eta_1 = \eta_2 = 0.12$, $\omega_c/2\pi = 2.2$ GHz, $g_1 = 0.30\omega_c$, $g_2 = 0.49\omega_c$, $\varepsilon_1 = \varepsilon_2 = 0.01\omega_c$, $\Delta_1 = 2.78\omega_c$, and $\Delta_2 = 4.94\omega_c$.

$t_1 + \pi/2G_{m1}^{(0)}(0, 0.12) \approx 0.0338\,\mu s$. The next step involves tuning the driving frequency to $\omega = \Delta_2(0, 0)$, which results in the state $|\psi(t_3)\rangle = (|2,0\rangle - i|0,1\rangle)/\sqrt{2}$ after the time $t_3 = t_2 + \pi/2G_{m2}^{(0)}(0, 0.12) \approx 0.0640\,\mu s$. Ultimately, when the driving frequency $\omega = \Delta_2(0, 1)$ is satisfied, the quantum state becomes $|\psi(t_4)\rangle = (|2,0\rangle + |0,2\rangle)/\sqrt{2}$ at the moment $t_4 = t_3 + \pi/2G_{m2}^{(0)}(1, 0.12) \approx 0.0854\,\mu s$. In addition, we have applied the Gaussian soft control to the system, and the fidelity of the target quantum state can be found through Table II. To further investigate the generation of the magnon NOON state [70,71], we conduct simulations to assess the fidelity for larger total qubit numbers N_1 and N_2. On the right panel of Fig. 7, it is evident to hold high fidelity as the two total qubit numbers increase. Notably, when $N_1 = N_2 = 1 \times 10^3$, the fidelity value can reach $F = 0.9644$. The feasibility of the NOON state has been established by us. Strictly speaking, the effective $G_{mj}^{(0)} \propto \epsilon_j \sqrt{N_j}$, as indicated by the effective Hamiltonian in Eq. (25). When the number of atoms becomes sizable, a significant coupling strength emerges, and validity of the effective Hamiltonian should be examined. To avoid undesired transitions, an appropriate number of qubits N_j and ϵ_j should be considered, ensuring that the high-frequency vibration term can be safely disregarded. By doing so, we can achieve a series of desired entangled states with high fidelity.

V. DECOHERENCE AND EXPERIMENTAL FEASIBILITY

In this section, we first provide a detailed analysis when the system suffers from decoherence, considering scenarios with both a few and a large number of qubits. Subsequently, we present experimentally feasible parameters for implementing our proposed scheme.

A. Decoherence of the dynamic system

In order to better discuss the scheme we have proposed, we now describe the system dynamics by considering the dissipation channels taken into account. Here, we employ a dressed-state master equation by considering that the standard master
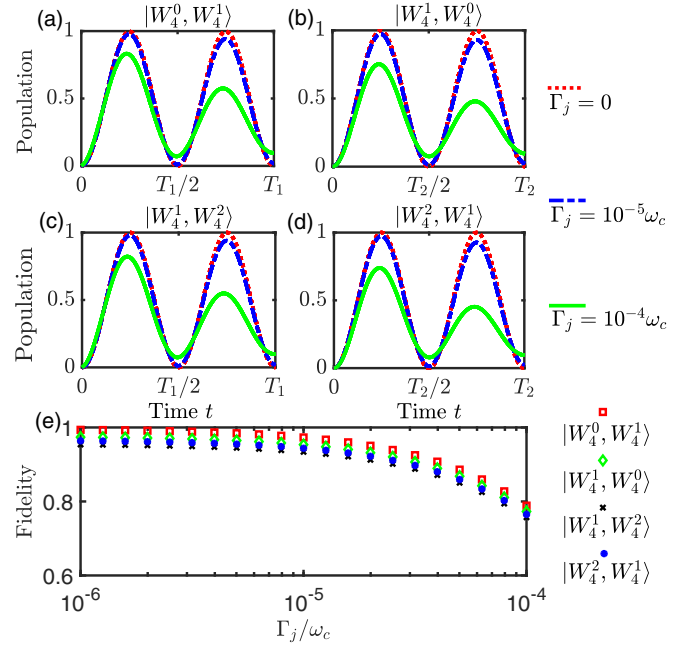

FIG. 8. [(a)–(d)] Dynamic evolution of the target state $|W_4^0, W_4^1\rangle$, $|W_4^1, W_4^0\rangle$, $|W_4^2, W_4^1\rangle$, and $|W_4^1, W_4^2\rangle$ starting from the initial state $|W_4^1, W_4^1\rangle$ under various dissipative processes. (e) Fidelity of the target state evolving half a period under different dissipation conditions. The dynamics is governed by the Hamiltonian in Eq. (28). The parameter $\kappa = 10^{-5}\omega_c$ and other parameters are consistent with those shown in Fig. 2.

equation breaks down in the ultrastrong coupling regime [72,73]. With the Born-Markov approximation and assuming each qubit ensemble suffering collective dissipation [74–76], the dressed-state master equation at zero temperature reads

$$\frac{d\hat{\rho}}{dt} = -i[\hat{H}, \hat{\rho}] + \sum_{m,n>m} \left(\Gamma_{q_1}^{nm} + \Gamma_{q_2}^{nm} + \Gamma_c^{nm} \right) \mathcal{D}[|m\rangle\langle n|]\hat{\rho},$$

(28)

where the Lindblad operator $\mathcal{D}[\hat{O}]\hat{\rho} = 2\hat{O}\hat{\rho}\hat{O}^\dagger - \hat{\rho}\hat{O}^\dagger\hat{O} - \hat{O}^\dagger\hat{O}\hat{\rho}$. $|m\rangle$ and $|n\rangle$ are eigenstates of the undriven (i.e., $A_j = 0$) Hamiltonian given by Eq. (1) with eigenvalues ω_m and ω_n. Here, the eigenstates are labeled by an increasing order (i.e., $\omega_n > \omega_m$ for $n > m$). The qubit ensembles and resonator decay rates can be written as

$$\Gamma_{q_j}^{nm} = \frac{\Gamma_j}{N_j} \frac{\Delta_{nm}}{\omega_{q_j}} |\langle m|\hat{S}_j^- + \hat{S}_j^+|n\rangle|^2,$$

$$\Gamma_c^{nm} = \kappa \frac{\Delta_{nm}}{\omega_c} |\langle m|\hat{a} + \hat{a}^\dagger|n\rangle|^2,$$

where κ and Γ_j are the bare loss rates for the resonator and the jth qubit ensemble, and $\Delta_{nm} = \omega_n - \omega_m$. To evaluate the robustness of the proposal, we introduce the definition of the fidelity as $F[|\psi_T\rangle, \rho(t)] = \langle\psi_T|\rho(t)|\psi_T\rangle$, with $\rho(t)$ being the evolution density matrix. In Figs. 8(a)–8(d), we depict the temporal dynamics of the selective transition under the dissipation. We consider an initial state $|W_4^1, W_4^1\rangle$ and assume $\Gamma_1 = \Gamma_2$ for convenience. In the ideal case when $\Gamma_j = 0$, coherent oscillations of the initial state and target

TABLE III. The fidelity of the corresponding target states is obtained with the initial state $|W_4^1, W_4^1\rangle$ under different dissipation rates. The dynamics is governed by the Hamiltonian in Eq. (28).

	$\Gamma_j = 0$	$\Gamma_j = 10^{-5}\omega_c$	$\Gamma_j = 10^{-4}\omega_c$
$|W_4^0, W_4^1\rangle$	0.9963	0.9778	0.8262
$|W_4^1, W_4^0\rangle$	0.9997	0.9749	0.7774
$|W_4^2, W_4^1\rangle$	0.9959	0.9735	0.7891
$|W_4^1, W_4^2\rangle$	0.9997	0.9794	0.8143

state occur, indicating that photon loss has minimal impact on the system. However, as the rate of dissipation increases, the coherence oscillations are destroyed by dissipation, and the fidelity of the target states is decreased. Figure 8(e) further shows the fidelity of the target state evolving half a period under different dissipation rates. Table III shows that with an increase in the dissipation, the accuracy of the target state diminishes. Nonetheless, the results show that the selective transition can be achieved under dissipative processes, and the Dicke states can be created within the coherent time.

In the thermodynamic limit $N_j \gg 1$, we show the resulting coupling scales as $\epsilon_j \sqrt{N_j}$. However, we emphasize that this previous approximation can be highly effective even in the more practical scenario of a finite number of atoms, specifically, when the number of excitations in the system is significantly less than the total number N_j of atoms in the ensemble. Hence, when $\Gamma_1 = \Gamma_2$ and $N_1 = N_2$, the dressed-state master equation can be obtained by Holstein-Primakoff transformation [75]. Consequently, the dressed-state master equation after Holstein-Primakoff transformation can be recast as

$$\frac{d\hat{\tilde{\rho}}}{dt} = -i[\hat{\tilde{H}}, \hat{\tilde{\rho}}] + \sum_{m,n>m} (\tilde{\Gamma}_{q_1}^{nm} + \tilde{\Gamma}_{q_2}^{nm} + \tilde{\Gamma}_c^{nm}) \mathcal{D}[|\tilde{m}\rangle\langle\tilde{n}|]\hat{\tilde{\rho}}.$$

(29)

Here, the tilde indicates symbols after Holstein-Primakoff transformation, and $|\tilde{m}\rangle$ and $|\tilde{n}\rangle$ are eigenstates of the undriven Hamiltonian given by Eq. (1) after Holstein-Primakoff transformation with eigenvalues $\tilde{\omega}_m$ and $\tilde{\omega}_n$. The resonator and qubit ensembles decay rates associated with the given system can be written as

$$\tilde{\Gamma}_{q_j}^{nm} = \Gamma_j \frac{\tilde{\Delta}_{nm}}{\omega_{q_j}} |\langle\tilde{m}|\hat{m}_j + \hat{m}_j^\dagger|\tilde{n}\rangle|^2,$$

$$\tilde{\Gamma}_c^{nm} = \kappa \frac{\Delta_{nm}}{\omega_c} |\langle\tilde{m}|\hat{a} + \hat{a}^\dagger|\tilde{n}\rangle|^2,$$

where $\tilde{\Delta}_{nm} = \tilde{\omega}_n - \tilde{\omega}_m$. In Fig. 9, we show the evolution of the target state under the different dissipative rates, revealing a similar trend to the previous scenario with a noticeable decrease in the fidelity of the target state as the dissipation rate increases. Additionally, we provide the corresponding fidelity values in the presence of decoherence, which aligns perfectly with the aforementioned results. These results highlight the high robustness of the entire system under lower levels of dissipation. Furthermore, Table IV illustrates that as dissipa-
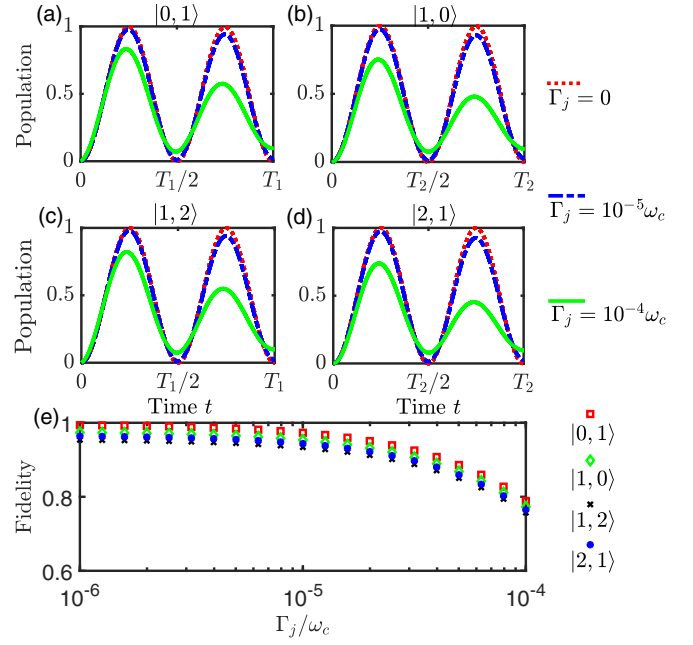

FIG. 9. [(a)–(d)] Dynamic evolution process of the target state $|0, 1\rangle$, $|1, 0\rangle$, $|1, 2\rangle$, and $|2, 1\rangle$ starting from the initial state $|1, 1\rangle$ under dissipative processes. (e) Fidelity of the final state and target state. The dynamics is governed by the Hamiltonian in Eq. (29). The parameter $\kappa = 10^{-5}\omega_c$ and other selected parameters are consistent with those shown in Fig. 6.

tion increases, the accuracy of the target state diminishes, and coherence gradually decreases over time.

B. Experimental consideration and feasibility

To assess the feasibility of our entangled Dicke states generation scheme in a realistic experiment, we now discuss the relevant achievable experimental parameters. As outlined in the main text, our protocol works in the ultrastrong light-matter coupling regime. For the case with few atoms, our proposal can be realized in circuit QED systems. In such superconducting circuit experiments, qubit and resonator frequencies are usually in the range $\omega_{c,(q_j)}/2\pi \sim$ 1–10 GHz [77–79]. The coupling strengths range from $g/\omega_c \simeq 0.12$ to theoretical limits $g/\omega_c \sim$ 1–3 for flux qubits [80,81]. In this work, we choose $\omega_c/2\pi = 2.2$ GHz, $\omega_{q_1}/2\pi = 2.87\omega_c \simeq$ 6.31 GHz, and $\omega_{q_2}/2\pi = 2.87\omega_c \simeq$ 10.87 GHz. We choose $g_1/\omega_c = 0.25$ and $g_2/\omega_c = 0.49$. Thus, the physical parameters of the scheme are accessible in current technologies.

TABLE IV. The fidelity of the corresponding target states is obtained with the initial state $|1, 1\rangle$ under different dissipation conditions. The dynamics is governed by the Hamiltonian in Eq. (29).

	$\Gamma_j = 0$	$\Gamma_j = 10^{-5}\omega_c$	$\Gamma_j = 10^{-4}\omega_c$
$|0, 1\rangle$	0.9953	0.9775	0.7961
$|1, 0\rangle$	0.9986	0.9745	0.7448
$|2, 1\rangle$	0.9951	0.9729	0.7525
$|1, 2\rangle$	0.9984	0.9783	0.7838

Recent experimental work has also demonstrated that dissipation and dephasing rates in a flux qubit are of the order of $2\pi \times 10$ kHz [82–84]. For transmission-line resonators, quality factors on the order of 10^6 have been realized [85], which indicates that quantum coherence of systems is of the order of 1–10 ms within current experimental capabilities [86]. For the large number of two-level systems, our proposal can also be studied with a hybrid system consisting of qubit ensembles and a superconducting resonator [87]. Each qubit ensemble can be realized using the NV centers in a diamond crystal, and each qubit ensemble is coupled to a superconducting resonator placed between these two qubit ensembles. The coupling strengths between the resonator and qubit ensembles can be tuned in to ultrastrong coupling regimes by either engineering the hybrid structure in advance or tuning the excitation frequencies of qubit ensembles via the external magnetic fields.

VI. CONCLUSION

In conclusion, we have presented a scheme for entangling two Dicke states in a periodic modulated system. The effectiveness of this method can be verified through numerical simulations. For some special cases, the ensemble-ensemble entangled state can be obtained by means of an even-odd cat states projective measurement. Additionally, Gaussian soft control can be utilized to enhance the fidelity of the target states. In the thermodynamics limit, our protocol can also be applied to attain the selective interactions between two distinct magnon systems by means of the Holstein-Primakoff transformation. Furthermore, it has successfully shown the creation of high-fidelity magnon states in a large number of qubits, which establishes a reliable approach for generating a magnon NOON state in the thermodynamic limit. Finally, in the presence of decoherence during dynamical evolution, our scheme can achieve highly reliable target entangled states. This provides further evidence for the experimental feasibility of our approach in preparing entangled states with high fidelity.

[1] L. S. Silveira and R. M. Angelo, Classical-hidden-variable description for entanglement dynamics of two-qubit pure states, Phys. Rev. A **95**, 062105 (2017).

[2] H. Zhu and M. Hayashi, General framework for verifying pure quantum states in the adversarial scenario, Phys. Rev. A **100**, 062335 (2019).

[3] Y.-F. Qiao, H.-Z. Li, X.-L. Dong, J.-Q. Chen, Y. Zhou, and P.-B. Li, Phononic-waveguide-assisted steady-state entanglement of silicon-vacancy centers, Phys. Rev. A **101**, 042313 (2020).

[4] P. Contreras-Tejada, C. Palazuelos, and J. I. deVicente, Asymptotic survival of genuine multipartite entanglement in noisy quantum networks depends on the topology, Phys. Rev. Lett. **128**, 220501 (2022).

[5] A. Morvan, L. Chen, J. M. Larson, D. I. Santiago, and I. Siddiqi, Optimizing frequency allocation for fixed-frequency superconducting quantum processors, Phys. Rev. Res. **4**, 023079 (2022).

[6] A. Eddins, M. Motta, T. P. Gujarati, S. Bravyi, A. Mezzacapo, C. Hadfield, and S. Sheldon, Doubling the size of quantum simulators by entanglement forging, PRX Quantum **3**, 010309 (2022).

[7] D. Alsina and J. I. Latorre, Experimental test of Mermin inequalities on a five-qubit quantum computer, Phys. Rev. A **94**, 012314 (2016).

[8] Z.-E. Su, W.-D. Tang, D. Wu, X.-D. Cai, T. Yang, L. Li, N.-L. Liu, C.-Y. Lu, M. Żukowski, and J.-W. Pan, Experimental test of the irreducible four-qubit Greenberger-Horne-Zeilinger paradox, Phys. Rev. A **95**, 030103(R) (2017).

[9] M.-X. Luo and S.-M. Fei, Robust multipartite entanglement without entanglement breaking, Phys. Rev. Res. **3**, 043120 (2021).

[10] T. Orito, Y. Kuno, and I. Ichinose, Quantum information spreading in random spin chains with topological order, Phys. Rev. B **106**, 104204 (2022).

[11] C. A. González-Gutiérrez and J. M. Torres, Atomic Bell measurement via two-photon interactions, Phys. Rev. A **99**, 023854 (2019).

[12] J. D. Wong-Campos, S. A. Moses, K. G. Johnson, and C. Monroe, Demonstration of two-atom entanglement with ultrafast optical pulses, Phys. Rev. Lett. **119**, 230501 (2017).

[13] T. Seidelmann, C. Schimpf, T. K. Bracht, M. Cosacchi, A. Vagov, A. Rastelli, D. E. Reiter, and V. M. Axt, Two-photon excitation sets limit to entangled photon pair generation from quantum emitters, Phys. Rev. Lett. **129**, 193604 (2022).

[14] Z. M. E. Chaisson, P. F. Poitras, M. Richard, Y. Castonguay-Page, P.-H. Glinel, V. Landry, and D. R. Hamel, Phase-stable source of high-quality three-photon polarization entanglement by cascaded down-conversion, Phys. Rev. A **105**, 063705 (2022).

[15] X.-L. Wang, L.-K. Chen, W. Li, H.-L. Huang, C. Liu, C. Chen, Y.-H. Luo, Z.-E. Su, D. Wu, Z.-D. Li, H. Lu, Y. Hu, X. Jiang, C.-Z. Peng, L. Li, N.-L. Liu, Y.-A. Chen, C.-Y. Lu, and J.-W. Pan, Experimental ten-photon entanglement, Phys. Rev. Lett. **117**, 210502 (2016).

[16] A. C. Tzemos and G. Contopoulos, Ergodicity and Born's rule in an entangled three-qubit Bohmian system, Phys. Rev. E **104**, 054211 (2021).

[17] M. Kounalakis, G. E. W. Bauer, and Y. M. Blanter, Analog quantum control of magnonic cat states on a chip by a superconducting qubit, Phys. Rev. Lett. **129**, 037205 (2022).

[18] Y. Wang, Y. Li, Z.-q. Yin, and B. Zeng, 16-qubit IBM universal quantum computer can be fully entangled, npj Quantum Inf. **4**, 46 (2018).

[19] Z. Hou, H.-S. Zhong, Y. Tian, D. Dong, B. Qi, L. Li, Y. Wang, F. Nori, G.-Y. Xiang, C.-F. Li, and G.-C. Guo, Full reconstruction of a 14-qubit state within four hours, New J. Phys. **18**, 083036 (2016).

[20] T. Monz, P. Schindler, J. T. Barreiro, M. Chwalla, D. Nigg, W. A. Coish, M. Harlander, W. Hänsel, M. Hennrich, and R. Blatt, 14-qubit entanglement: Creation and coherence, Phys. Rev. Lett. **106**, 130506 (2011).

[21] C. Song, K. Xu, W. Liu, C.-p. Yang, S.-B. Zheng, H. Deng, Q. Xie, K. Huang, Q. Guo, L. Zhang, P. Zhang, D. Xu, D. Zheng, X. Zhu, H. Wang, Y.-A. Chen, C.-Y. Lu, S. Han, and J.-W. Pan, 10-qubit entanglement and parallel logic operations with a superconducting circuit, Phys. Rev. Lett. **119**, 180511 (2017).

[22] F. Kranzl, M. K. Joshi, C. Maier, T. Brydges, J. Franke, R. Blatt, and C. F. Roos, Controlling long ion strings for quantum simulation and precision measurements, Phys. Rev. A **105**, 052426 (2022).

[23] W.-X. Guo, Y.-K. Wu, Y.-Y. Huang, L. Feng, C.-X. Huang, H.-X. Yang, J.-Y. Ma, L. Yao, Z.-C. Zhou, and L.-M. Duan, Picosecond ion-qubit manipulation and spin-phonon entanglement with resonant laser pulses, Phys. Rev. A **106**, 022608 (2022).

[24] G.-Z. Song, M.-J. Tao, J. Qiu, and H.-R. Wei, Quantum entanglement creation based on quantum scattering in one-dimensional waveguides, Phys. Rev. A **106**, 032416 (2022).

[25] S. J. Masson and S. Parkins, Extreme spin squeezing in the steady state of a generalized Dicke model, Phys. Rev. A **99**, 023822 (2019).

[26] J. K. Stockton, R. van Handel, and H. Mabuchi, Deterministic Dicke-state preparation with continuous measurement and control, Phys. Rev. A **70**, 022106 (2004).

[27] M. T. Johnsson, N. R. Mukty, D. Burgarth, T. Volz, and G. K. Brennen, Geometric pathway to scalable quantum sensing, Phys. Rev. Lett. **125**, 190403 (2020).

[28] H. Hakoshima and Y. Matsuzaki, Efficient detection of inhomogeneous magnetic fields from a single spin with Dicke states, Phys. Rev. A **102**, 042610 (2020).

[29] Y.-C. Liu, X.-D. Yu, J. Shang, H. Zhu, and X. Zhang, Efficient verification of Dicke states, Phys. Rev. Appl. **12**, 044020 (2019).

[30] G. Tóth, Multipartite entanglement and high-precision metrology, Phys. Rev. A **85**, 022322 (2012).

[31] L. Pezzè, A. Smerzi, M. K. Oberthaler, R. Schmied, and P. Treutlein, Quantum metrology with nonclassical states of atomic ensembles, Rev. Mod. Phys. **90**, 035005 (2018).

[32] R. H. Dicke, Coherence in spontaneous radiation processes, Phys. Rev. **93**, 99 (1954).

[33] J.-F. Huang and L. Tian, Modulation-based superradiant phase transition in the strong-coupling regime, Phys. Rev. A **107**, 063713 (2023).

[34] Y.-F. Xiao, X.-B. Zou, and G.-C. Guo, Generation of atomic entangled states with selective resonant interaction in cavity quantum electrodynamics, Phys. Rev. A **75**, 012310 (2007).

[35] R. Prevedel, G. Cronenberg, M. S. Tame, M. Paternostro, P. Walther, M. S. Kim, and A. Zeilinger, Experimental realization of Dicke states of up to six qubits for multiparty quantum networking, Phys. Rev. Lett. **103**, 020503 (2009).

[36] X.-Q. Shao, L. Chen, S. Zhang, Y.-F. Zhao, and K.-H. Yeon, Deterministic generation of arbitrary multi-atom symmetric Dicke states by a combination of quantum Zeno dynamics and adiabatic passage, Europhys. Lett. **90**, 50003 (2010).

[37] A. K. Ekert, Quantum cryptography based on Bell's theorem, Phys. Rev. Lett. **67**, 661 (1991).

[38] C.-H. Wang, K. Noh, J. Lebreuilly, S. M. Girvin, and L. Jiang, Photon-number-dependent Hamiltonian engineering for cavities, Phys. Rev. Appl. **15**, 044026 (2021).

[39] Y. Q. Ji, Y. L. Liu, S. J. Zhou, X. M. Xiu, L. Dong, H. K. Dong, Y. J. Gao, and X. X. Yi, Fast conversion of Dicke states $|D_n^{(2)}\rangle$ to $|D_{n+1}^{(2)}\rangle$ by transitionless quantum driving, Phys. Rev. A **99**, 023808 (2019).

[40] Y.-L. Liu, Y.-Q. Ji, X. Han, W.-X. Cui, S. Zhang, and H.-F. Wang, Fast conversion of three-particle Dicke states to four-particle Dicke states with Rydberg superatoms, Adv. Quantum Technol. **6**, 2200173 (2023).

[41] Z. Li, B. Braverman, S. Colombo, C. Shu, A. Kawasaki, A. F. Adiyatullin, E. Pedrozo-Peñafiel, E. Mendez, and V. Vuletić, Collective spin-light and light-mediated spin-spin interactions in an optical cavity, PRX Quantum **3**, 020308 (2022).

[42] Z. Zhang and L. M. Duan, Quantum metrology with Dicke squeezed states, New J. Phys. **16**, 103037 (2014).

[43] I. Apellaniz, B. Lücke, J. Peise, C. Klempt, and G. Tóth, Detecting metrologically useful entanglement in the vicinity of Dicke states, New J. Phys. **17**, 083027 (2015).

[44] D.-Y. Wang, C.-H. Bai, S. Liu, S. Zhang, and H.-F. Wang, Dissipative bosonic squeezing via frequency modulation and its application in optomechanics, Opt. Express **28**, 28942 (2020).

[45] P. Jung, Periodically driven stochastic systems, Phys. Rep. **234**, 175 (1993).

[46] V. Novičenko, E. Anisimovas, and G. Juzeliūnas, Floquet analysis of a quantum system with modulated periodic driving, Phys. Rev. A **95**, 023615 (2017).

[47] N. Yu, S. Wang, C. Sun, and G. Wang, Switchable selective interactions in a Dicke model with driven biased term, Phys. Rev. E **105**, 034125 (2022).

[48] L. Cong, S. Felicetti, J. Casanova, L. Lamata, E. Solano, and I. Arrazola, Selective interactions in the quantum Rabi model, Phys. Rev. A **101**, 032350 (2020).

[49] X.-Q. Shao, Selective Rydberg pumping via strong dipole blockade, Phys. Rev. A **102**, 053118 (2020).

[50] T. Neuman, M. Trusheim, and P. Narang, Selective acoustic control of photon-mediated qubit-qubit interactions, Phys. Rev. A **101**, 052342 (2020).

[51] F. Mu, Y. Gao, H. Yin, and G. Wang, Dicke state generation via selective interactions in a Dicke-Stark model, Opt. Express **28**, 39574 (2020).

[52] C. Wu, C. Guo, Y. Wang, G. Wang, X.-L. Feng, and J.-L. Chen, Generation of Dicke states in the ultrastrong-coupling regime of circuit QED systems, Phys. Rev. A **95**, 013845 (2017).

[53] C. Wu, Y. Wang, C. Guo, Y. Ouyang, G. Wang, and X.-L. Feng, Initializing a permutation-invariant quantum error-correction code, Phys. Rev. A **99**, 012335 (2019).

[54] S.-I. Chu and D. A. Telnov, Beyond the Floquet theorem: Generalized Floquet formalisms and quasienergy methods for atomic and molecular multiphoton processes in intense laser fields, Phys. Rep. **390**, 1 (2004).

[55] S.-K. Son, S. Han, and S.-I. Chu, Floquet formulation for the investigation of multiphoton quantum interference in a superconducting qubit driven by a strong ac field, Phys. Rev. A **79**, 032301 (2009).

[56] X. Luo, J. Huang, H. Zhong, X. Qin, Q. Xie, Y. S. Kivshar, and C. Lee, Pseudo-parity-time symmetry in optical systems, Phys. Rev. Lett. **110**, 243902 (2013).

[57] P. Hänggi, P. Talkner, and M. Borkovec, Reaction-rate theory: Fifty years after Kramers, Rev. Mod. Phys. **62**, 251 (1990).

[58] A. Eckardt and E. Anisimovas, High-frequency approximation for periodically driven quantum systems from a Floquet-space perspective, New J. Phys. **17**, 093039 (2015).

[59] J. F. Haase, Z.-Y. Wang, J. Casanova, and M. B. Plenio, Soft quantum control for highly selective interactions among joint quantum systems, Phys. Rev. Lett. **121**, 050402 (2018).

[60] T. Holstein and H. Primakoff, Field dependence of the intrinsic domain magnetization of a ferromagnet, Phys. Rev. **58**, 1098 (1940).

[61] M. Kitagawa and M. Ueda, Squeezed spin states, Phys. Rev. A **47**, 5138 (1993).

[62] J.-F. Huang, J.-Q. Liao, L. Tian, and L.-M. Kuang, Manipulating counter-rotating interactions in the quantum Rabi model via modulation of the transition frequency of the two-level system, Phys. Rev. A **96**, 043849 (2017).

[63] J. Zhou, Y. Hu, X.-B. Zou, and G.-C. Guo, Ground-state preparation of arbitrarily multipartite Dicke states in the one-dimensional ferromagnetic spin-$\frac{1}{2}$ chain, Phys. Rev. A **84**, 042324 (2011).

[64] D. B. Hume, C. W. Chou, T. Rosenband, and D. J. Wineland, Preparation of Dicke states in an ion chain, Phys. Rev. A **80**, 052302 (2009).

[65] A. Tameshtit and J. E. Sipe, Evolution of coherences and populations in the secular approximation, Phys. Rev. A **49**, 89 (1994).

[66] C. E. Creffield, Location of crossings in the Floquet spectrum of a driven two-level system, Phys. Rev. B **67**, 165301 (2003).

[67] D. S. Schlegel, F. Minganti, and V. Savona, Quantum error correction using squeezed Schrödinger cat states, Phys. Rev. A **106**, 022431 (2022).

[68] S. Izumi, M. Takeoka, K. Wakui, M. Fujiwara, K. Ema, and M. Sasaki, Projective measurement onto arbitrary superposition of weak coherent state bases, Sci. Rep. **8**, 2999 (2018).

[69] X. Q. Shao, F. Liu, X. W. Xue, W. L. Mu, and W. Li, High-fidelity interconversion between Greenberger-Horne-Zeilinger and w states through Floquet-Lindblad engineering in Rydberg atom arrays, Phys. Rev. Appl. **20**, 014014 (2023).

[70] J. P. Dowling, Quantum optical metrology – The lowdown on high-N00N states, Contemp. Phys. **49**, 125 (2008).

[71] S.-f. Qi and J. Jing, Generating NOON states in circuit QED using a multiphoton resonance in the presence of counter-rotating interactions, Phys. Rev. A **101**, 033809 (2020).

[72] F. Beaudoin, J. M. Gambetta, and A. Blais, Dissipation and ultrastrong coupling in circuit QED, Phys. Rev. A **84**, 043832 (2011).

[73] A. Settineri, V. Macrí, A. Ridolfo, O. Di Stefano, A. F. Kockum, F. Nori, and S. Savasta, Dissipation and thermal noise in hybrid quantum systems in the ultrastrong-coupling regime, Phys. Rev. A **98**, 053834 (2018).

[74] L. Song and J. Jin, Crossover from discontinuous to continuous phase transition in a dissipative spin system with collective decay, Phys. Rev. B **108**, 054302 (2023).

[75] V. Macrì, F. Nori, S. Savasta, and D. Zueco, Spin squeezing by one-photon–two-atom excitation processes in atomic ensembles, Phys. Rev. A **101**, 053818 (2020).

[76] J. Gelhausen, M. Buchhold, and P. Strack, Many-body quantum optics with decaying atomic spin states: (γ, κ) Dicke model, Phys. Rev. A **95**, 063824 (2017).

[77] F. Yoshihara, T. Fuse, S. Ashhab, K. Kakuyanagi, S. Saito, and K. Semba, Characteristic spectra of circuit quantum electrodynamics systems from the ultrastrong- to the deep-strong-coupling regime, Phys. Rev. A **95**, 053824 (2017).

[78] F. Yoshihara, T. Fuse, S. Ashhab, K. Kakuyanagi, S. Saito, and K. Semba, Superconducting qubit–oscillator circuit beyond the ultrastrong-coupling regime, Nat. Phys. **13**, 44 (2017).

[79] Y.-H. Chen, W. Qin, R. Stassi, X. Wang, and F. Nori, Fast binomial-code holonomic quantum computation with ultrastrong light-matter coupling, Phys. Rev. Res. **3**, 033275 (2021).

[80] T. Niemczyk, F. Deppe, H. Huebl, E. P. Menzel, F. Hocke, M. J. Schwarz, J. J. Garcia-Ripoll, D. Zueco, T. Hümmer, E. Solano, A. Marx, and R. Gross, Circuit quantum electrodynamics in the ultrastrong-coupling regime, Nat. Phys. **6**, 772 (2010).

[81] G. Romero, D. Ballester, Y. M. Wang, V. Scarani, and E. Solano, Ultrafast quantum gates in circuit QED, Phys. Rev. Lett. **108**, 120501 (2012).

[82] P. Forn-Díaz, L. Lamata, E. Rico, J. Kono, and E. Solano, Ultrastrong coupling regimes of light-matter interaction, Rev. Mod. Phys. **91**, 025005 (2019).

[83] M. Stern, G. Catelani, Y. Kubo, C. Grezes, A. Bienfait, D. Vion, D. Esteve, and P. Bertet, Flux qubits with long coherence times for hybrid quantum circuits, Phys. Rev. Lett. **113**, 123601 (2014).

[84] J.-L. Orgiazzi, C. Deng, D. Layden, R. Marchildon, F. Kitapli, F. Shen, M. Bal, F. R. Ong, and A. Lupascu, Flux qubits in a planar circuit quantum electrodynamics architecture: Quantum control and decoherence, Phys. Rev. B **93**, 104518 (2016).

[85] H. Paik, D. I. Schuster, L. S. Bishop, G. Kirchmair, G. Catelani, A. P. Sears, B. R. Johnson, M. J. Reagor, L. Frunzio, L. I. Glazman, S. M. Girvin, M. H. Devoret, and R. J. Schoelkopf, Observation of high coherence in Josephson junction qubits measured in a three-dimensional circuit QED architecture, Phys. Rev. Lett. **107**, 240501 (2011).

[86] A. Megrant, C. Neill, R. Barends, B. Chiaro, Y. Chen, L. Feigl, J. Kelly, E. Lucero, M. Mariantoni, P. J. J. O'Malley, D. Sank, A. Vainsencher, J. Wenner, T. C. White, Y. Yin, J. Zhao, C. J. Palmstrøm, J. M. Martinis, and A. N. Cleland, Planar superconducting resonators with internal quality factors above one million, Appl. Phys. Lett. **100**, 113510 (2012).

[87] Y. Qiu, W. Xiong, L. Tian, and J. Q. You, Coupling spin ensembles via superconducting flux qubits, Phys. Rev. A **89**, 042321 (2014).